Clim. Past Discuss., 2, 1249–1276, 2006
www.clim-past-discuss.net/2/1249/2006/

Climate of the Past Discussions

Climate of the Past Discussions is the access reviewed discussion forum of *Climate of the Past*

Simulated northern hemispheric storm tracks of the Eemian interglacial and the last glacial inception

F. Kaspar, T. Spangehl, and U. Cubasch

Freie Universität Berlin, Institut für Meteorologie, Berlin, Germany

Received: 16 November 2006 – Accepted: 27 November 2006 – Published: 7 December 2006

Correspondence to: F. Kaspar (frank.kaspar@met.fu-berlin.de)

Abstract

Climate simulations of the Eemian interglacial and the last glacial inception have been performed by forcing a coupled ocean-atmosphere general circulation model with insolation patterns of these periods. The parameters of the Earth's orbit have been set to conditions of 125 000 and 115 000 years before present (yr BP). Compared to today, these dates represent periods with enhanced and weakened seasonality of insolation on the northern hemisphere. Here we analyze the simulated change in winter storm tracks. The change in the orbital configuration has a strong impact on the meridional temperature gradients and therefore on strength and location of the storm tracks. The North Atlantic storm track is strenghtened, shifted northward and extends further to the east in the simulation for the Eemian at 125 kyr BP. As one consequence, the northern parts of Europe experience an increase in winter precipitation. The frequency of winter storm days increases over large parts of the North Atlantic. Opposite but weaker changes in storm track activity are simulated for 115 kyr BP.

1 Introduction

Climate variations during the last 500 000 years are dominated by interglacial-glacial-cycles, which are believed to be driven by changes in insolation as a result of variations in Earth's orbit around the sun (Berger, 1988). Palaeoclimatic records reveal that interglacials occurred approximately every 100 000 years in this period and lasted for 7000 to 17 000 years. Here, we present simulations of the Eemian interglacial, which was the last interglacial before the present one (approx. 130 000 yr BP–116 000 yr BP; Kukla et al., 2002). The simulations approximately represent periods with maximum and minimum summer insolation on the northern hemisphere. These periods are connected with different states of the climate system that are visible in palaeodata, namely: The minimum of global ice volume occurred at approx. 125 000 yr BP. We therefore consider this date as representative for the warm phase of the Eemian (hereafter: EEM).

CPD

2, 1249–1276, 2006

After ca. 115 000 yr BP, open vegetation replaced forests in northwestern Europe and at Vostok air temperatures dropped sharply (Kukla et al., 2002). We use this date to represent the start of the last glaciation (hereafter: GI, "glacial inception"). Three parameters are responsible for the seasonal distribution of insolation: the eccentricity of the Earth's orbit, the angle of the axis of rotation (obliquity) and the position of the equinoxes relative to the perihelion. The combined effect of greater obliquity and eccentricity, together with the fact that perihelion occurred in northern hemisphere summer caused an amplification of the northern hemispheric seasonal cycle of insolation at 125 000 yr BP. At 65° North the insolation at mid-month June was 11.7% higher than today (531 W/m^2 instead of 475 W/m^2). The insolation of mid-month December was 1.9 W/m^2 compared to 3.0 W/m^2 today. At 115 000 yr BP the angle of perihelion was almost opposite compared to 125 000 yr BP and similar to today. The perihelion occurring in northern hemisphere winter combined with greater eccentricity and lower obliquity caused a weakening of the seasonal cycle of insolation on the northern hemisphere. The insolation of mid-month June at 65° North was 7.6% lower (439 W/m^2) than today. At mid-month December it was 6.8 W/m^2. For a detailed discussion of insolation patterns during interglacials see Berger et al. (2006). Although absolute changes in insolation on the northern hemisphere are strongest in summer, northern high latitudinal winter temperatures can also be strongly modified due to indirect effects, as for example via the influence of oceanic or atmospheric dynamics or changes in sea-ice distribution. Therefore, the changed orbital configuration could lead to distinct changes in the seasonal cycle of temperature, especially over land. Due to the temperature gradients and the occurence of baroclinic waves in the midlatitudes, present-day winter climate is characterized by the occurence of cyclones and anticyclones, which play a major role in transferring energy from the equator to the poles. The associated fronts are largely responsible for extremes in precipitation and wind at these latitudes. Regions of high frequent variability in mean sea level pressure or geopotential height have been intensively studied for observed present-day climate (Blackmon, 1976; Blackmon et al., 1977) as well as in model-based climate change projections for the 21st century.

"Storm tracks" defined after Blackmon et al. (1977) as regions with large synoptic-scale activity can be calculated as the standard deviation of the band-pass filtered geopotential height and are often used to quantify baroclinic wave activity. General circulation models are able to simulate the present-day storm tracks fairly well (e.g. Stendel and Roeckner, 1998; Hall et al., 1996). As these models also indicate significant changes in storm tracks under climate change scenarios (Yin, 2005), it is of interest to evaluate the ability of the models to simulate storm tracks under different conditions. Kageyama et al. (1999) analyzed storm tracks in a number of GCMs for the last glacial maximum at 21 kyr BP. At that time orbital configuration was similar to today, but climate was strongly influenced by the presence of large ice sheets and differences in sea surface temperatures. Nearly all models reacted with an eastward shift of the storm tracks. Hall and Valdes (1997) analyzed winter storm tracks in a GCM simulation for 6000 years before present, also a period with enhanced summer insolation on the northern hemisphere. They found an increase in baroclinicity for the storm tracks of the Atlantic and the Pacific.

In this article, we analyze storm tracks in simulations of the Eemian interglacial and the subsequent glacial inception. The climate model and the setup of the experiments are described in Sect. 2. In Sect. 3 we give an overview over some general features of the simulations and present the results for the northern hemispheric winter storm tracks and related climatic parameters. In Sect. 4 the results are discussed and compared with simulations of future climate change.

2 Model description and experimental setup

2.1 The ECHO-G model

The ECHO-G model (Legutke and Maier-Reimer, 1999; Legutke and Voss, 1999) consists of the ECHAM4 atmosphere model (Roeckner et al., 1992) coupled to the HOPE-G ocean model. The atmospheric component is a spectral model with a horizontal re-

solution of T30 (≈3.75°) and 19 vertical hybrid sigma-pressure levels with the highest level at 10 hPa. The ocean model HOPE-G is the global version of the Hamburg Ocean Primitive Equation Model (Wolff et al., 1997) and includes a dynamic-thermodynamic sea-ice model with a viscous-plastic rheology (Hibler, 1979). A gaussian T42 Arakawa E-Grid (≈2.8°) is used with a gradual meridional refinement reaching 0.5° in the tropical ocean between 10° S and 10° N. The vertical resolution is given by 20 horizontal levels with eight levels within the top 2000 m from the ocean surface. The atmospheric and oceanic components are coupled with a flux correction. The model time steps are 30 min for ECHAM4 and 12 h for HOPE-G. The resolution of the model is appropriate for palaeoclimatic experiments as it allows to simulate time-slices of several centuries on modern computing facilities. The analysis of a 1000-year control simulation shows an overall good skill in simulating today's climatology and interannual variability (Min et al., 2005a). The El Niño Southern Oscillation (ENSO) and the North Atlantic Oscillation (NAO) are also simulated reasonably well (Min et al., 2005b). Stendel and Roeckner (1998) showed that the spatial resolution of T30 in ECHAM4 is sufficient for the representation of synoptic cyclones and that storm tracks are simulated in satisfactorily agreement with ERA-15 reanalysis data. Fischer-Bruns et al. (2005) analyzed midlatitude storm activity based on wind speed thresholds in ECHO-G simulations with historical and climate change forcing. They found a poleward shift in the climate change experiments and increasing activity over the North Atlantic.

2.2 The experiments

The simulations are performed as equilibrium experiments with constant boundary conditions. Therefore the simulated temporal climate variations are only caused by the nonlinear internal dynamics of the climate model. The orbital parameters and greenhouse gas concentrations have been set to values of 125 kyr BP and 115 kyr BP (hereafter EEM and GI). Orbital parameters have been calculated according to Berger (1978). Greenhouse gas concentrations (CO_2, CH_4, N_2O) have been adapted to values obtained from Vostok ice cores (Petit et al., 1999; Sowers, 2001). Concentrations

of chlorofluorocarbons (CFCs) are set to zero. The model's default values are retained for all the remaining boundary conditions, i.e. present-day conditions are used. A third simulation with preindustrial conditions is used for comparison (hereafter PI). We did not select a present-day simulation, as greenhouse gas concentrations of the preindustrial simulation are very similar to the values in the Eemian and therefore the simulated anomalies can be attributed more clearly to insolation change. All parameters are shown in Table 1. All simulations have been initialized with the same oceanic state, i.e. potential temperature and salinity calculated from the Levitus et al. (1994) climatology.

3 Results

3.1 General behaviour of the simulations

The simulations have been performed for at least 2000 years. During the first ≈100 years all simulations are dominated by similar initial trends that are related to adaptions of the ocean circulation. In this period global mean near surface temperature rises by approx. 0.4 K. Most features of the oceanic circulation reach quasi-stationary conditions after approx. 150 years in all three simulations. After this initial phase the simulations of the preindustrial and the Eemian climate are relativly stable. In the simulation for 115 kyr BP a significant long-term cooling trend occurs which is connected with an expansion of perennial snow-covered areas over northern parts of North America and an increase in northern hemispheric sea ice volume. A detailed description of general features of these simulations can be found in Kaspar and Cubasch (2006).

For the further analysis we selected a interval of 100 years during the early part of the simulations starting 300 years after the beginning of the simulations. This period was selected, because the simulations have already reached their equilibrium, but the perennial snow-covered areas over North America are still very limited. Therefore the structure of the temperature patterns are mainly influenced by the orbital configuration. Anomalies are shown relative to the same interval of the preindustrial simulation.

The changed seasonality of insolation leads to a modification of the high latitudinal temperature gradients. These are decisive for strength and location of the storm tracks. Summer temperatures directly react to the strong changes of the high northern insolation, i.e. they are significantly higher for 125 000 yr BP and significanly lower for 115 000 yr BP. This temperature change is especially strong on the continental areas. In contrast to that, winter temperatures are mainly influenced by indirect effect. Winter insolation is reduced at 125 000 yr BP, leading to reduced temperatures over North America and the lower northern latitudes (compared to the preindustrial simulation). However, temperatures are higher in large parts of the Arctic sea, as a result of reduced sea ice coverage (Fig. 1). Temperatures are especially increased in north-east Europe. In that region increased advection of oceanic heat due to stronger westerly winds leads to a strong winter warming. The simulated seasonal temperature patterns over Europe are in good agreement with pollen-based temperature reconstructions (Kaspar et al., 2005).

For 115 000 yr BP winter insolation was increased. However, the temperatures of the Arctic sea are reduced, as they are dominated by the influence of the increased sea ice coverage (Fig. 2). Increased temperatures occur in a region in the north-west of the North Atlantic. This effect is caused by an enhanced North Atlantic current in this simulation, which is caused by the stronger meridional temperature gradient.

3.2 Winter storm tracks in the preindustrial simulation

Following Blackmon (1976), storm tracks are often quantified by the variability of the bandpass (typically 2.5–6 or 2.5–8 days) filtered geopotential height (GPH) fields at 500 hPa. Alternatively the calculation of storm tracks can be based on sea level pressure (SLP). Here we used a Butterworth bandpass filter (Hoffmann, 1999) with cut-off periods of 2.5 and 8 days and applied it to the time series of the 12-hourly SLP and GPH (at 500 hPa) fields. Based on this filtered time series we calculated the standard deviation for the winter seasons (DJF). Storm tracks are then represented by the regions with high values of this standard deviation.

Figure 3 shows the results for the preindustrial simulation. The maximum of the SLP-based Atlantic storm track is located at around 53° W and 52° N. The maximum of the Pacific storm track is located at around 175° E and 48° N (SLP). The location of the storm track is quite well reproduced compared to ECMWF re-analyses data (see for example Kageyama et al., 1999). When storm tracks are calculated based on geopotential height (at 500 hPa) the maximum lies approx. 5° further south (Fig. 4).

3.3 Winter storm tracks during the Eemian

Figure 5 shows the winter storm tracks in the simulation for 125 kyr BP as differences from the preindustrial simulation. The figure indicates a significant northward shift of the Atlantic storm track. The region with activity greater than 700 Pa also extends further eastward. In a large region around the maximum of the North Atlantic storm track at around 60° N changes exceed 50 Pa. Storm track activity is also enhanced over the North American continent, including Alaska. The Pacific storm track is weakened mainly in its western part (120° E to 180° E). Its eastern part in the region of Alaska is shifted northward. Over the Asian continent the activity is reduced, as well as over the Mediterranean region (by about more than 20 Pa over large areas). When the analysis is done based on geopotential height at 500 hPa, the spatial distribution of the anomalies is similar but more zonally oriented (Fig. 6). Anomalies exceed 6 gpm over the Atlantic. The weakening of the Pacific storm track is more distinct in this case.

The main reasons for the simulated changes are the differences in the meridional temperature gradients. Reduced winter temperatures over the high latitudes of the western part of the North Atlantic and North America are responsible for a stronger temperature gradient in this region at 125 kyr BP, resulting in an enhanced storm track activity. Especially over the North Atlantic this results in a northward shift of the storm tracks. Over the Mediterranean region the winter temperature gradient is reduced compared to the preindustrial case for two reasons: Over Northern Africa, reduced winter temperatures are simulated mainly because of reduced insolation. Over north-eastern Europe higher winter temperatures are caused by enhanced westerly winds

CPD
2, 1249–1276, 2006

EGU

and reduced sea-ice coverage. Hence, reduced storm track activity is simulated for the Mediterranean region. For Asia a temperature reduction is simulated for the southern part, whereas slightly higher temperatures occur in the Arctic sea. In combination, the merdional temperature gradient over Asia is reduced and consequently a reduced strom track activity is simulated for the northern part of the continent (north of 50° N).

At 115 kyr BP the change in storm track activity is approx. complementary compared to 125 kyr BP, but not as strong (Fig. 7). The Atlantic storm track is shifted slightly southward and has a reduced strength especially at its eastern part. The reduction is about >20 Pa east of 30° E. Storm track activity over the north-western parts of North America is reduced by a similar amount. The Pacific storm track activity is increased at its eastern part, whereas the change over Asia is relatively small. A distinct increase of activity also occurs in an area extending from the eastern Mediterranean to approx. 75° E. Again, the anomalies have a stronger zonal structure when calculated based on geopotential height at 500 hPa (not shown).

The strong changes over North America are related to the temperature changes caused by the increased sea ice coverage in the Arctic. The southward shift of the Atlantic storm track is caused by the increased temperatures over the western part of the North Atlantic. The relatively weak changes over Asia are due to the fact, that temperature changes over Asia are also comparatively small. The temperature decrease over the Arctic ocean close to Siberia does not result in a significant modification of storm track activity over Asia.

3.4 Change in extreme wind speed and precipitation

Storm tracks are closely related to other climatic parameters that could be relevant for the interpretation of paleoclimatic data, as for example precipitation or the number of storm days. These two will be discussed in this section.

The frequency of extreme wind events is an alternative possibility to measure storm activity. Fischer-Bruns et al. (2005) analyzed storm activity of an ECHO-G simulation by counting the number of winter days reaching or exceeding a minimum wind speed

within a grid box. As threshold they used the lower limit of the WMO Beaufort wind speed scale of 8 Bft (17.2 ms^{-1}). Here we apply the same method and threshold.

As Fig. 8 indicates for the preindustrial case, the area where this wind speed is exceeded is almost solely restricted to the oceans. A value of 50 storm days for the winter season (DJF) is exceeded in a small region over the Atlantic as well as over the Pacific. The maximum over the Atlantic is located at 37° W/47° N. Over the Pacific it is located at 175° W/40° N.

The change of the frequency of winter storm days is shown in Fig. 9 for the EEM simulation. The North Atlantic north of 45° N is affected by an increase in the frequency, with the strongest changes in the eastern part at around 55° N. The increase in this region in the neighbourhood of the British Isles is of about 6 storm days, which is an increase of around 20% compared to the preindustrial simulation (Fig. 8). The European coastal regions from France to Norway are affected by an increase of at least 2 storm days. A belt with a reduced number of storm days is visible at around 30° N. In total, the changes on the North Atlantic indicate a northward shift of the regions with frequent storm days. This is consistent with the northward shift of the storm tracks described in the previous section. The results for the Pacific also reflect the pattern of changes in storm track activity.

In case of the GI simulation (Fig. 10) the general structure of the changes are also in consistency with the changes of the storm tracks. On the eastern Atlantic the frequency is reduced between latitudes 35° N and 70° N. The decrease reaches 4 days in some areas. The western part of the North Atlantic is affected by an increase in storm frequency (north of 30° N). A northward shift of the frequency occurs over the Pacific.

The Figs. 11 and 12 show the simulated change of winter precipitation for EEM and GI as ration to the preindustrial simulation. A strong change in precipitation is visible for those regions of the North Atlantic and Europe that are affected by the described changes in storm track activity. In case of the EEM simulation, a large region is affected by a precipitation increase of around 10%. The region includes Iceland, the British Isles and Scandinavia. It includes the European continent north of 55° N and extends up to

CPD
2, 1249–1276, 2006

EGU

80° N.

In case of the GI simulation the European continent does not experience strong changes in precipitation. Changes related to the storm tracks occur in the eastern North Atlantic (Fig. 12).

4 Summary and conclusions

Anomalies of northern hemispheric winter storm tracks as a measure for synoptic-scale activity have been analyzed for simulations with orbital forcing of two phases of the Eemian interglacial: The Eemian warm phase at 125 kyr BP and the subsequent glacial inception at 115 kyr BP. The stongest simulated change in storm track activity occured in the simulation for 125 kyr BP namely a significant northward shift of the North Atlantic storm track, combined with an increase in activity. The frequency of storm days has been used to identify regions with intense storm activity. As with that measure similar regions of strongest change have been identified, it can be concluded that this is a robust conclusion. One caveat is that the results are only based on one single coupled model.

The results showed, that the changes in storm tracks can be explained with changes in the meridional winter temperature gradients. For Europe these simulated changes in the temperature gradient have been compared with proxy-data in an earlier study (Kaspar et al., 2005). In that study it has been shown that the simulated seasonal patterns of the temperature anomalies are in good agreement with pollen-based reconstructions. We therefore assume that changes in temperature gradients are simulated realistically and can therefore also assume that the spatial patterns of changes in storm tracks are simulated realistically.

The question whether the Eemian could be used as analog for a warmed future climate has been a matter of debate (see for example Mearns et al., 2001). Analyses of storm tracks with GCMs under greenhouse gas scenarios show similiar spatial patterns in storm tracks than simulated here for the Eemian at 125 kyr BP: Bengtsson

et al. (2006) found a similar distribution of changes for a future climate change scenario: indications for a northward shift, a weakening of the Mediterranean storm track and a strengthening north of the British Isles (for IPCC-SRES-scenario A1B). These pattern agrees with the findings in Sect. 3.3 (cmp. also Fig. 5). Yin (2005) analyzed an ensemble of 21st century simulations performed by 15 coupled climate models and also found a poleward shift and intensification of the northern hemispheric winter storm track simulated by all but four models (for IPCC-SRES-scenario A1B).

Fischer-Bruns et al. (2005) calculated the frequency of storm days for an ECHO-G climate change simulation (for IPCC-SRES scenario A2). Again, the simulated change in frequency of winter storm days shows a similar structure and order of magnitude as simulated here for the Eemian, with strongest changes in the neighbouring regions of the British Isles. In summary, the results suggest that concerning the shift of winter storm tracks the Eemian interglacial reveals a similar signal than future climate scenarios. For 115 kyr BP the changes are of opposite sign, but less strong.

Changes in North Atlantic storm tracks lead to changes in European precipitation. This information could be relevant for the interpretation of paleoclimatic proxies. Our results suggest that an increase in winter precipitation does mainly occur in the northern parts of Europe at 125 kyr BP (north of 55° N). For southern Europe and for 115 kyr BP the changes in winter precipitation are comparatively small.

Acknowledgements. This work has been performed within the German Climate Research Program DEKLIM of the German Ministry for Education and Research (BMBF). The simulations have been run on the NEC SX-6 supercomputer of the German Climate Computing Centre (DKRZ, Hamburg).

References

Blackmon, M. L.: A climatological spectral study of the 500 mb geopotential height of the Northern Hemisphere, J. Atmos. Sci., 33, 1607–1623, 1976. 1251, 1255

Blackmon, M. L., Wallace, J. M., Lau, N.-C., and Mullen, S. J.: An observational study of the northern hemisphere wintertime circulation, J. Atmos. Sci., 34, 1040–1053, 1977. 1251, 1252

Bengtsson, L., Hodges, K. I., and Roeckner, E.: Storm tracks and climate change, J. Climate, 19, 3518–3543, 2006. 1259

Berger, A. L.: Long-term variations of daily insolation and Quarternary climate changes, J. Atmos. Sci., 35, 2362–2367, 1978. 1253, 1264

Berger, A. L.: Milankovitch theory and climate, Rev. Geophys., 26, 624–657, 1988. 1250

Berger, A. L., Loutre, M.-F., Kaspar, F., and Lorenz, S. J.: Insolation during interglacials, in: The Climate of Past Interglacials, edited by: Sirocko, F., Litt, T., Claussen, M., and Sánchez-Goñi, M. F., Developments in Quaternary Sciences, volume 7, Elsevier, in press, 2006. 1251

Fischer-Bruns, I., von Storch, H., Gonzáles-Rouco, J. F., and Zorita, E.: Modelling the variabiliy of midlatitude storm activity on decadel to century time scales, Clim. Dyn., 25(5), 461–476, 2005. 1253, 1257, 1260

Hall, N. M., Dong, B., and Valdes, P. J.: Atmospheric equilibrium, instability and energy transport at the last glacial maximum, Clim. Dyn., 12, 497–511, 1996. 1252

Hall, N. M. and Valdes, P. J.: A GCM simulation of the climate 6000 years ago, J. Climate, 10, 3–17, 1997. 1252

Hibler III, W. D.: A dynamic thermodynamic sea ice model, J. Phys. Oceanogr., 9, 817–846, 1979. 1253

Hoffmann, G.: Die Bedeutung der diabatischen Heizung für die synoptische Störungsaktivität der Nordhemisphäre im heutigen und in einem zukünftigen Klima, Mitteilungen aus dem Institut für Geophysik und Meteorologie der Universität zu Köln, Heft 126, 1999. 1255

Kageyama, M., Valdes, P. J., Ramstein, G., Hewitt, C., and Wyputta, U.: Northern hemisphere storm tracks in present day and last glacial maximum climate simulations: A comparison of the European PMIP models, J. Climate, 12, 742–760, 1999. 1252, 1256

Kaspar, F. and Cubasch, U.: Simulations of the Eemian interglacial and the subsequent glacial inception with a coupled ocean-atmosphere general circulation model, in: The Climate of Past Interglacials, edited by: Sirocko, F., Litt, T., Claussen, M., and Sánchez-Goñi, M. F., Developments in Quaternary Sciences, volume 7, Chapter 33, Elsevier, in press, 2006. 1254

Kaspar, F., Kühl, N., Cubasch, U., and Litt, T.: A model-data-comparison of European temperatures in the Eemian interglacial, Geophys. Res. Lett., 32, L11703, doi:10.1029/2005GL022456, 2005. 1255, 1259

Kukla, G. J., Bender, M. L., de Beaulieu, J. L., Bond, G., Broecker, W. S., Cleveringa, P., Gavin, J. E., Herbert, T. D., Imbrie, J., Jouzel, J., Keigwin, L. D., Knudsen, K. L., McManus, J. F., Merkt, J., Muhs, D. R., and Müller, H.: Last Interglacial Climates, Quart. Res., 58, 2–13, 2002. 1250, 1251

Legutke, S. and Maier-Reimer, E.: Climatology of the HOPE-G Global Ocean – Sea Ice General Circulation Model, Technical Report 21, Deutsches Klimarechenzentrum, Hamburg, Germany, 1999. 1252

Legutke, S. and Voss, R.: The Hamburg Atmosphere-Ocean Coupled Circulation Model ECHO-G, Technical Report 18, Deutsches Klimarechenzentrum, Hamburg, 1999. 1252

Levitus, S., Burgett, R., and Boyer, T. P.: World Ocean Atlas. Vol. 3, Salinity and Vol. 4, Temperature. NOAA Atlas NESDIS 3/4, U.S. Government Printing Office, Washington, D.C., 1994. 1254

Mearns, L. O., Hulme, M., Carter, T. R., Leemans, R., Lal, M., and Whetton, P.: Climate Scenario Development, in: Climate Change 2001: The Scientific Basis, edited by: Houghton, J. T., Ding, Y., Griggs, D. J., et al., Chapter 13, pp. 739–768, Cambridge University Press, New York, 2001. 1259

Min, S.-K., Legutke, S., Hense, A., and Kwon, W.-T.: Internal variability in a 1000-year control simulation with the coupled climate model ECHO-G. Part I: near surface temperature, precipitation, and mean sea level pressure, Tellus A, 57(4), 605–621, 2005a. 1253

Min, S.-K., Legutke, S., Hense, A., and Kwon, W.-T.: Internal variability in a 1000-year control simulation with the coupled climate model ECHO-G. Part II: ENSO and NAO, Tellus A, 57(4), 622–640, 2005b. 1253

Petit, J. R., Jouzel, J., Raynaud, D., Barkov, N. I., Barnola, J. M., Basile, I., Bender, M., Chapellaz, J., Davis, J., Delaygue, G., Delmotte, M., Kotlyakov, V. M., Legrand, M., Lipenkov, V. M., Lorius, C., Pepin, L., Ritz, C., Saltzman, E., and Stievenard, M.: Climate and atmospheric history of the past 420.000 years from the Vostok ice core, Nature, 399, 429–436, 1999. 1253, 1264

Roeckner, E., Arpe, K., Bengtsson, L., Brinkop, S., Dümenil, L., Esch, M., Kirk, E., Lunkeit, F., Ponater, M., Rockel, B., Sausen, R., Schlese, U., Schubert, S., and Windelband, M.: Simulation of the present-day climate with the ECHAM model: Impact of model physics and resolution, Report No. 93, Max-Planck-Institute for Meteorology, Hamburg, Germany, 1992. 1252

Sowers, T.: N_2O record spanning the penultimate deglaciation from the Vostok ice core, J.

Geophys. Res.-Atmos., 106(D23), 31 903–31 914, 2001. 1253, 1264
Stendel, M. and Roeckner, E.: Impacts of horizontal resolution on simulated climate statistics in ECHAM4, Report No. 253, Max-Planck-Institute for Meteorology, Bundesstr. 55, Hamburg, Germany, 1998. 1252, 1253
Wolff, J. O., Maier-Reimer, E., and Legutke, S.: The Hamburg Ocean Primitive Equation Model HOPE. Technical Report No. 13, Deutsches Klimarechenzentrum, Hamburg, Germany, 1997. 1253
Yin, J. H.: A consistent poleward shift of the storm tracks in simulations of 21st century climate, Geophys. Res. Lett., 32, L18701, doi:10.1029/2005GL023684, 2005. 1252, 1260

Table 1. Orbital parameters and greenhouse gas concentrations of the simulations. Orbital parameters are calculated following Berger (1978). The angle of perihelion refers to vernal equinox. Greenhouse gas concentrations are based on Vostok ice cores (CO_2 and CH_4: Petit et al., 1999; N_2O: Sowers, 2001).

	125 kyr BP EEM	115 kyr BP GI	preindust. PI
Eccentricity	0.0400	0.0414	0.0167
Obliquity [°]	23.79	22.41	23.44
Perihelion [°]	127.3	290.9	282.7
CO_2 [ppmv]	270	265	280
CH_4 [ppbv]	630	520	700
N_2O [ppbv]	260	270	265
CFCs [ppbv]	0	0	0

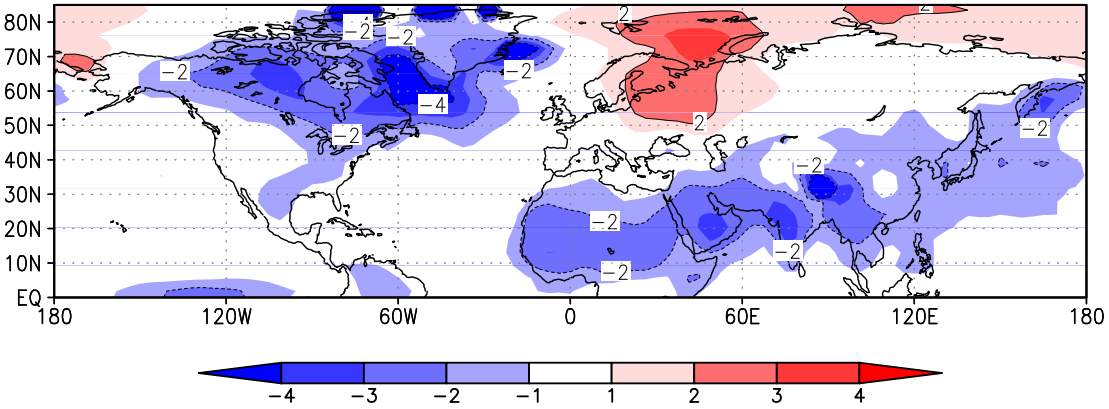

Fig. 1. Winter (DJF) temperature difference [K] between the EEM simulation and the PI simulation.

CPD
2, 1249–1276, 2006

Storm tracks of the Eemian and the last glacial inception

F. Kaspar et al.

EGU

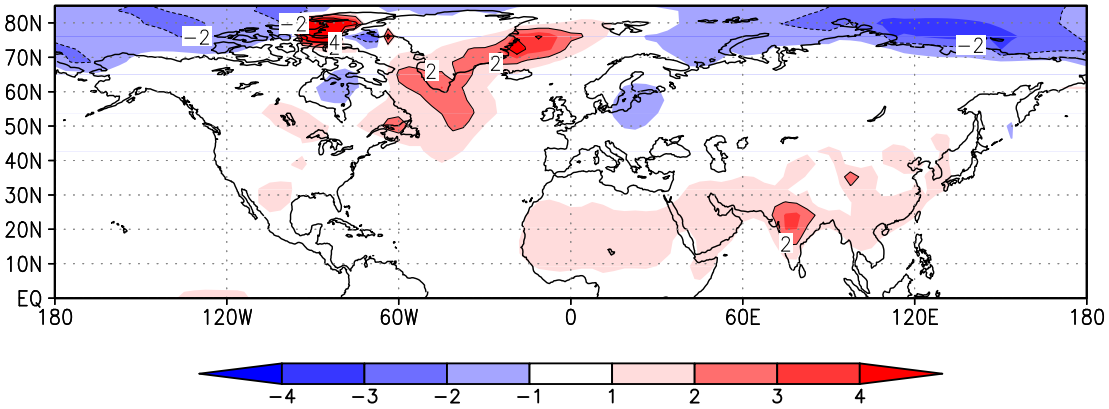

Fig. 2. Winter (DJF) temperature difference [K] between the GI simulation and the PI simulation.

CPD
2, 1249–1276, 2006

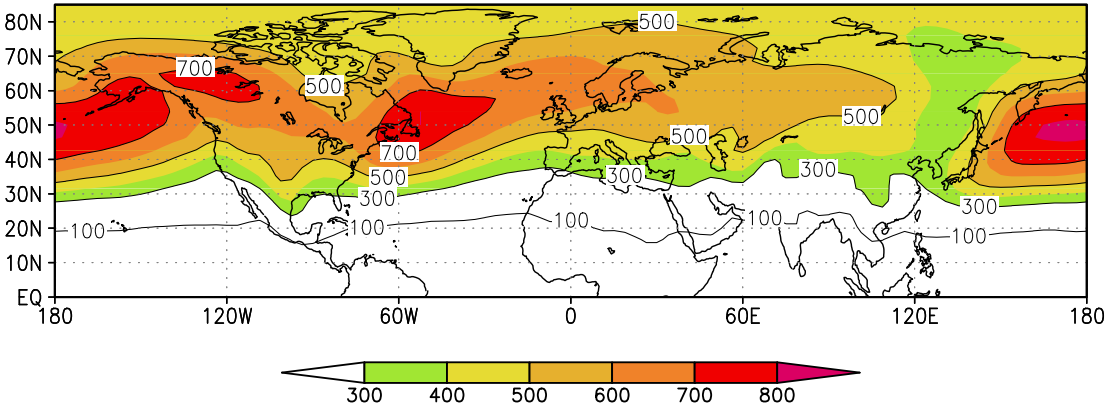

Fig. 3. Winter storm tracks of the preindustrial simulations [Pa], calculated as standard deviation of the filtered sea level pressure.

CPD
2, 1249–1276, 2006

EGU

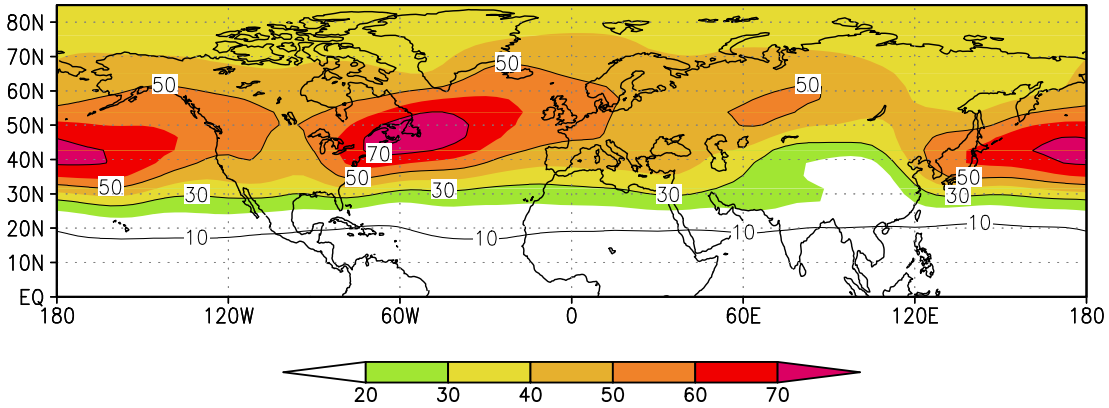

Fig. 4. Winter storm tracks of the preindustrial simulations [gpm], calculated as standard deviation of the filtered geopotential height at 500 hPa.

CPD
2, 1249–1276, 2006

EGU

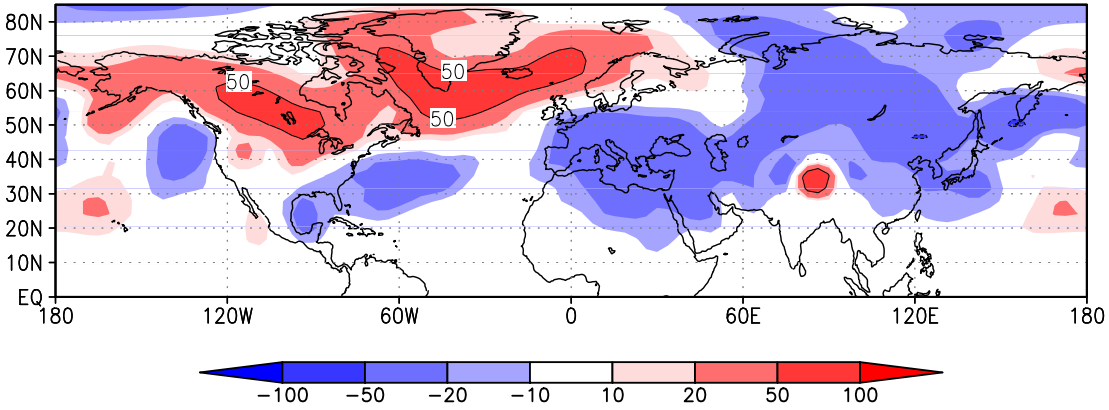

Fig. 5. Eemian winter storm track anomaly [Pa] at 125 kyr BP (EEM-PI) calculated based on sea level pressure as in Fig. 3.

CPD
2, 1249–1276, 2006

Storm tracks of the Eemian and the last glacial inception

F. Kaspar et al.

EGU

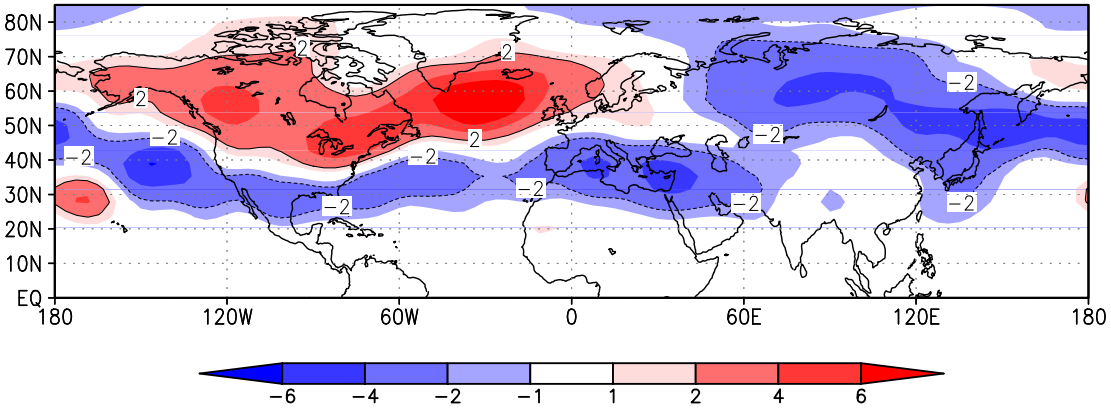

Fig. 6. Eemian winter storm track anomaly [gpm] at 125 kyr BP (EEM-PI) calculated based on geopotential height as in Fig. 4.

CPD
2, 1249–1276, 2006

Storm tracks of the Eemian and the last glacial inception

F. Kaspar et al.

EGU

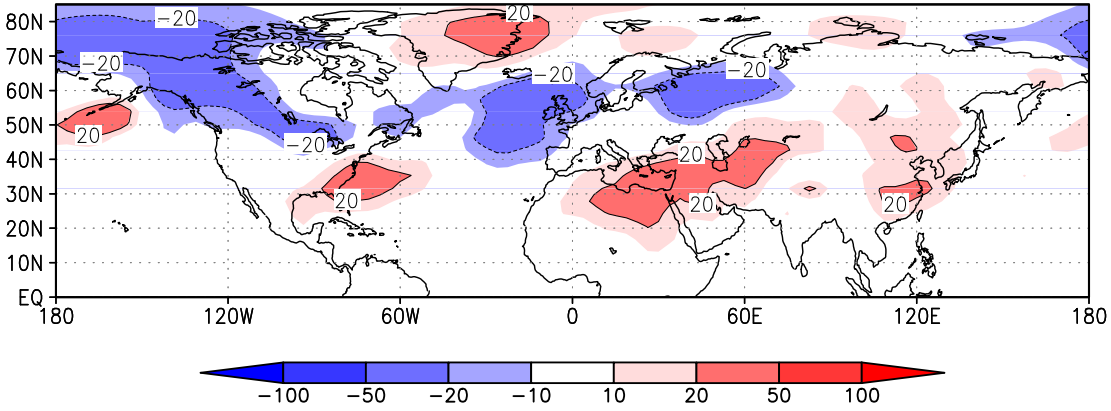

Fig. 7. Winter storm track anomaly [Pa] at 115 kyr BP (GI-PI) calculated based on sea level pressure as in Fig. 3.

CPD
2, 1249–1276, 2006

EGU

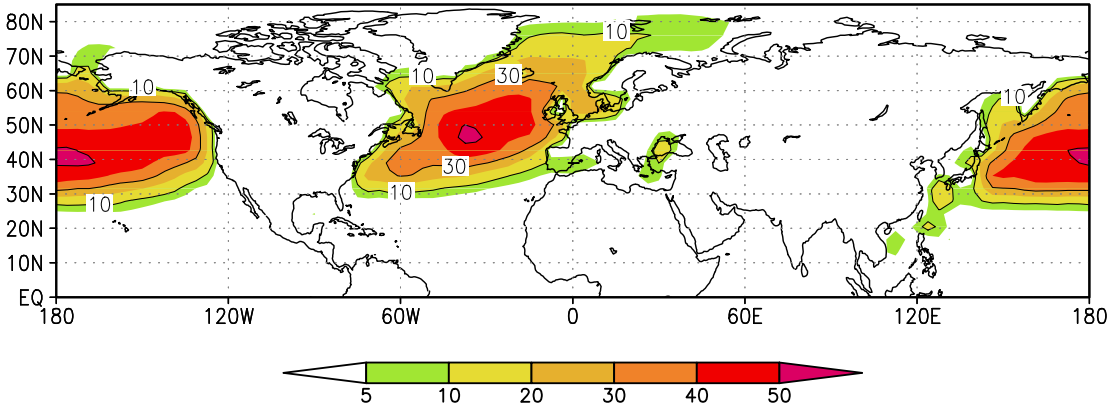

Fig. 8. Frequency of storm days (number of days with maximum daily 10 m wind speed reaching or exceeding the lower threshold of 8 Bft) for the winter season in the preindustrial simulation.

CPD
2, 1249–1276, 2006

EGU

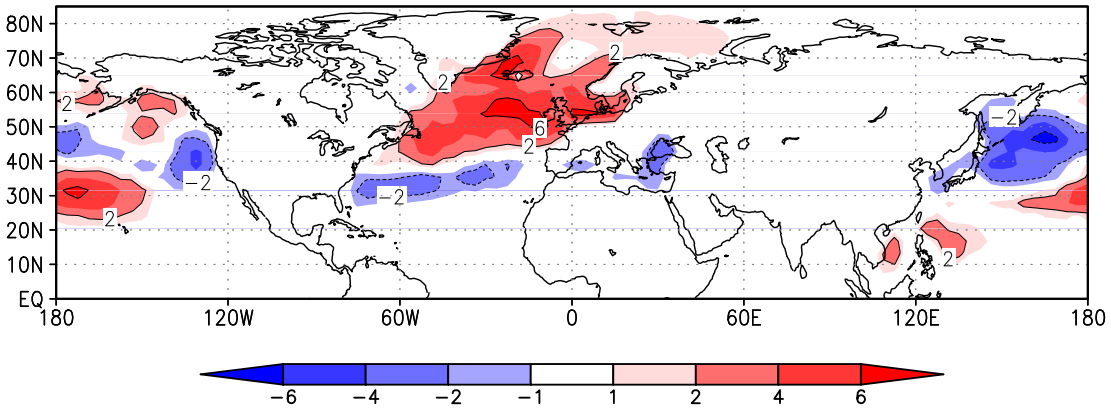

Fig. 9. Change in the number of storm days (defined as in Fig. 8) for the winter season in the simulation for 125 kyr BP (EEM-PI).

CPD
2, 1249–1276, 2006

EGU

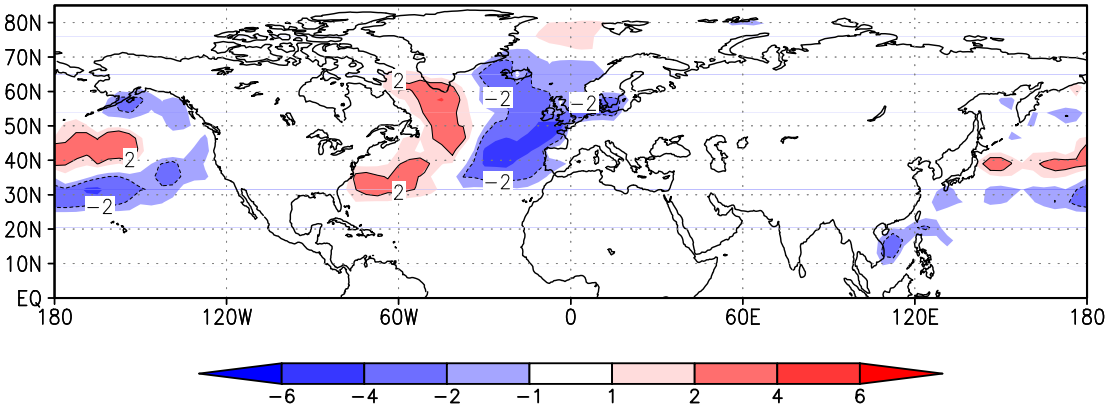

Fig. 10. Change in the number of storm days (defined as in Fig. 8) for the winter season in the simulation for 115 kyr BP (GI-PI).

CPD
2, 1249–1276, 2006

EGU

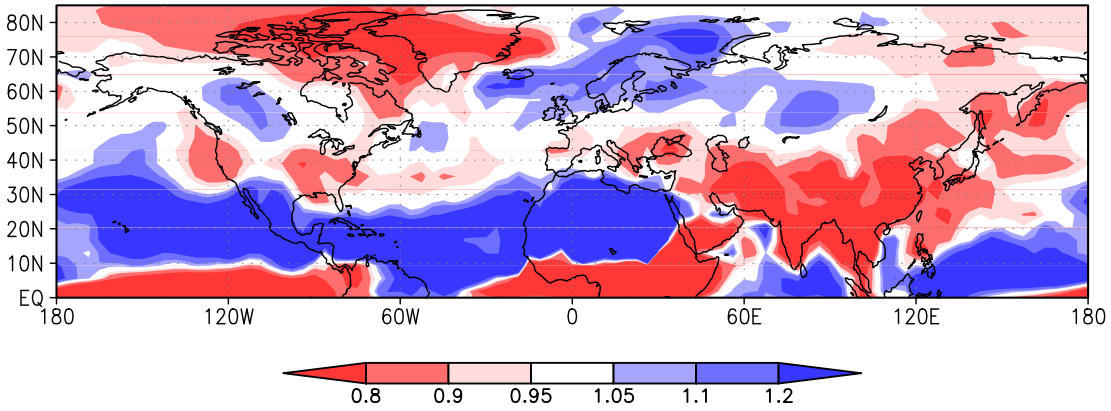

Fig. 11. Winter precipitation anomaly in the EEM simulation as ratio relative to the preindustrial simulation (EEM/PI).

CPD
2, 1249–1276, 2006

EGU

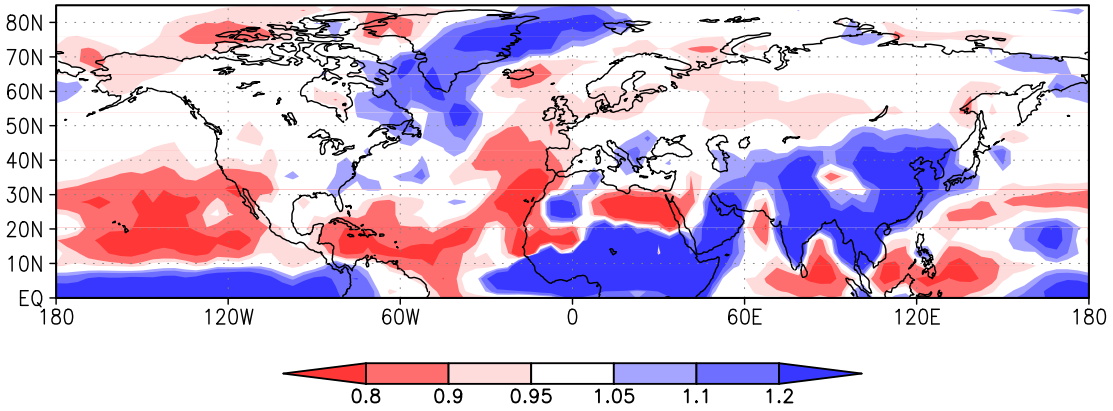

Fig. 12. Winter precipitation anomaly in the GI simulation as ratio relative to the preindustrial simulation (GI/PI).

CPD

2, 1249–1276, 2006

Storm tracks of the Eemian and the last glacial inception

F. Kaspar et al.

EGU